Localization of topological charge density near T_c in quenched QCD with Wilson flow

You-Hao Zou,* Jian-Bo Zhang,† and Guang-Yi Xiong‡
Department of Physics, Zhejiang University, Zhejiang 310027, People's Republic of China

(Received 21 May 2018; published 10 July 2018)

We smear quenched lattice QCD ensembles with lattice volume $32^3 \times 8$ by using Wilson flow. Six ensembles at temperature near the critical temperature T_c corresponding to the critical inverse coupling $\beta_c = 6.06173(49)$ are used to investigate the localization of topological charge density. If the effective smearing radius of Wilson flow is large enough, the density, size and peak of Harrington-Shepard (HS) caloron-like topological lumps of ensembles are stable when $\beta \leq 6.050$, but start to change significantly when $\beta \geq 6.055$. The inverse participation ratio (IPR) of topological charge density shows similar results, it begins to increase when $\beta \geq 6.055$ and is stable when $\beta \leq 6.050$. The pseudoscalar glueball mass is extracted from the topological charge density correlator (TCDC) of ensembles at $T = 1.19T_c$, and $1.36T_c$, the masses are 1.915(98) and 1.829(123) GeV respectively, they are consistent with results from conventional methods.

DOI: 10.1103/PhysRevD.98.014504

I. INTRODUCTION

Topological properties of the QCD vacuum are believed to play an important role in QCD. For example, the topological susceptibility has the famous Witten-Veneziano relation, which can explain the U(1) anomaly and the large mass of the η' meson [1–3]. The topological structure of the QCD vacuum is related to chiral symmetry breaking and may be also related to confinement [4,5].

A usual way to study the topological structure is investigating the localization of topological charge density, such as Belavin-Polyakov-Schwartz-Tyupkin (BPST) instanton-like localized topological lumps at zero temperature. BPST instanton is a semi-classical solution of the QCD Lagrangian in Euclidean space [6]. Isolated instantons are zero modes of the Dirac operator. When these modes mix with each other they will shift away from zero modes [5]. The way how they mix is important, since it is the topological structure of the QCD vacuum. When we use the gluonic definition for the topological charge density $q(x)$ to investigate the topological localized structures, such as instantons, a UV filter is needed to remove the short-ranged topological fluctuations and preserve the long-ranged topological structures [7–11].

Since the topological structure is connected with chiral symmetry breaking and confinement, we are interested in the behavior of topological structures when the temperature is near the critical temperature T_c. The temperature in lattice QCD is given by:

$$T = \frac{1}{N_t a_t}, \tag{1}$$

in which a_t is the lattice spacing in the temporal direction, and N_t is the temporal lattice size. Therefore we can change N_t or a_t to vary the temperature T. If we change N_t, because N_t cannot be too large the temperature will be changed coarsely. Thus we cannot get different ensembles with small variation of temperature near T_c. Therefore we will vary the temperature by changing a_t, which means that we will generate different temperature ensembles by slightly varying the inverse coupling β. The conventional UV filters like cooling, smoothing and smearing [12–16] lead to different smearing effects when the ensembles have different lattice spacings, even though the parameters are set to be the same. So we will use the gradient flow, which provides a general energy scale. Its effective smearing radius $\lambda = \sqrt{8t}$ [17], where t is the flow time. Recent works [18–20] show that the gradient flow is consistent with standard cooling, therefore like using cooling we can also use the gradient flow to study topological structures. Then we can compare the topological structure of different ensembles and avoid the different smearing effects.

In our work, we used the Harrington-Shepard (HS) caloron solutions [21] to filter the localized topological lumps, which is the generalized form of BPST instantons at

*11006067@zju.edu.cn
†jbzhang08@zju.edu.cn
‡xionggy@zju.edu.cn

finite temperature with periodic boundary condition at the temporal direction. We also used the inverse participation ratio (IPR) [22] to investigate the topological localization. The IPR is defined by:

$$\mathrm{IPR} = V\frac{\sum_x |q(x)|^2}{(\sum_x |q(x)|)^2}, \tag{2}$$

in which $q(x)$ is the topological charge density. In this work we use the gluonic definition for $q(x)$:

$$q(x) = \frac{1}{32\pi^2}\epsilon_{\mu\nu\rho\sigma}\mathrm{Tr}_C[F_{\mu\nu}(x)F_{\rho\sigma}(x)], \tag{3}$$

in which $\epsilon_{\mu\nu\rho\sigma}$ is the Levi-Civita symbol, Tr_C is the trace running over the color space, and the field tensor $F_{\mu\nu}$ is defined by:

$$F_{\mu\nu}(x) = -\frac{i}{2}(C_{\mu\nu}(x) - C^{\dagger}_{\mu\nu}(x)) - \frac{1}{3}\mathrm{ReTr}_C\left(-\frac{i}{2}(C_{\mu\nu}(x) - C^{\dagger}_{\mu\nu}(x))\right), \tag{4}$$

in which $C_{\mu\nu}(x)$ is the average of the four plaquettes on the $\mu-\nu$ plane. When all topological charges focus on one lattice site IPR $= V$, IPR would decrease if the topological charge density becomes more delocalized. Finally it will equal to 1 when the topological charge density distributes uniformly.

The topological charge density correlator (TCDC) of quenched QCD can be used to extract pseudoscalar glueball masses at zero temperature with Wilson flow [23]. In our work, we extracted the pseudoscalar glueball mass from TCDC at finite temperature with Wilson flow. The results are compared with those from Ref. [24]. Unlike conventional methods, this method does not need large lattice size in the temporal direction to do fitting, which is hard to be satisfied in ensembles at finite temperature especially at high temperatures.

II. LOCATING THE HS CALORON-LIKE TOPOLOGICAL LUMPS

A. Find the critical inverse coupling β_c

First, we need to find the critical temperature T_c. In other words we need to determine the critical inverse coupling β_c. We use pure gauge ensembles that have lattice size $32^3 \times 8$ in our work. We use the susceptibility χ_P of the Polyakov loop to find β_c. χ_P is defined as

$$\chi_P = \langle\Theta^2\rangle - \langle\Theta\rangle^2, \tag{5}$$

TABLE I. The quenched ensembles of Wilson action in this work. The lattice size is $32^3 \times 8$. 10000 sweeps were done before thermalization. Each configuration is separated by 10 sweeps. Each sweep includes 5 times quasi heat-bath and 5 steps of leapfrog.

β	N_{cnfg}	χ_P	a
6.045	2000	$3.02(38)\times10^{-4}$	0.0863 fm
6.050	2000	$4.92(14)\times10^{-4}$	0.0856 fm
6.055	2000	$7.67(23)\times10^{-4}$	0.0849 fm
6.060	2000	$9.36(47)\times10^{-4}$	0.0842 fm
6.065	2000	$8.15(19)\times10^{-4}$	0.0835 fm
6.070	2000	$5.82(18)\times10^{-4}$	0.0828 fm

in which Θ is the $Z(3)$ rotated Polyakov loop:

$$\Theta = \begin{cases} \mathrm{Re}P\exp[-2i\pi/3], & \arg P \in [\pi/3, \pi), \\ \mathrm{Re}P, & \arg P \in [-\pi/3, \pi/3), \\ \mathrm{Re}P\exp[2i\pi/3], & \arg P \in [-\pi, -\pi/3), \end{cases} \tag{6}$$

where P is the usual Polyakov loop of each configuration.

In Table I the 6 ensembles we used to find β_c are listed. The lattice size is $32^3 \times 8$. We expect that the finite volume effects are negligible. The lattice spacing a is found by using [25]

$$a = r_0\exp(-1.6804 - 1.7331(\beta-6) + 0.7849(\beta-6)^2 - 0.4428(\beta-6)^3), \tag{7}$$

where r_0 is set to be 0.5 fm from Ref. [26]. Obviously Table I shows that β_c is near 6.060. The critical inverse coupling β_c is obtained by interpolating to the location where χ_P is maximum. We use a B-spline interpolation and obtain $\beta_c = 6.06173(49)$, which is compatible with $\beta_c = 6.06239(38)$ in Ref. [27].

B. HS caloron-like topological lumps

In this paper we use the HS caloron solutions to filter the localized topological charge density lumps. The localized topological lumps are defined by sites that have maximum absolute value of $q(x_c)$ in a 3^4 hypercube centered at site x_c. The center x_c is also mentioned as peak. After applying the HS caloron filters in the following, we can get calorons-like topological lumps.

In SU(2) gauge theory at temperature T, HS caloron solution of gauge field $A_\mu(x)$ has the exact form as [21]

$$A_\mu(x) = A^a_\mu(x)T^a, \qquad T^a \text{ is the generators for SU(2)},$$
$$A^a_\mu(x) = \eta^{(\pm)}_{a\mu\nu}\partial_\nu \ln\Phi(x), \qquad \Phi(x) = 1 + \frac{\pi\rho^2}{|\vec{x}-\vec{x}_c|/T}\frac{\sinh(2T\pi|\vec{x}-\vec{x}_c|)}{\cosh(2T\pi|\vec{x}-\vec{x}_c|) - \cos(2T\pi(x_4 - x_{c4}))}, \tag{8}$$

where x_c is the center of a HS caloron, ρ is the size of a HS caloron. It satisfies the (anti-)self-dual condition $F_{\mu\nu} = \pm\tilde{F}_{\mu\nu}$, $\tilde{F}_{\mu\nu} = \frac{1}{2}\epsilon_{\mu\nu\rho\sigma}F_{\rho\sigma}$, $\eta^{(\pm)}_{a\mu\nu}$ is the 't Hooft symbol:

$$\eta^{(\pm)}_{a\mu\nu} = \epsilon_{a\mu\nu}, \quad \mu,\nu = 1,2,3,$$
$$\eta^{(\pm)}_{a4\nu} = -\eta^{(\pm)}_{a\nu4} = \pm\delta_{a\nu}, \quad \eta^{(\pm)}_{a44} = 0. \tag{9}$$

When the temperature $T \to 0$, it approaches the BPST instanton solution $\Phi(x) \to 1 + \frac{\rho^2}{(x-x_c)^2}$ [6]. Similar things happen when we constrain our study at the region $|x - x_c| \ll 1/T = N_t a_t$. Therefore when we use the center and its 8 closest neighbour sites on the lattice to filter the topological lumps with HS calorons, we can just use the BPST instanton solution to approximate the HS caloron solution in SU(3):

$$A^{a(\mathrm{BPST})}_{\mu}(x) = 2R^{a\alpha}\eta^{(\pm)}_{\alpha\mu\nu}\frac{(x-x_c)_\nu}{(x-x_c)^2}\frac{1}{1+\frac{(x-x_c)^2}{\rho^2}},$$
$$a = 1,2,\ldots,8, \qquad \alpha = 1,2,3, \tag{10}$$

where $R^{a\alpha}$ represents the color rotations embedding the SU(2) BPST instantons into SU(3).

The topological charge density near the center of an isolated instanton approximates

$$q^{\mathrm{BPST}}(x) = \pm\frac{6}{\pi^2\rho^4}\left(\frac{\rho^2}{(x-x_c)^2+\rho^2}\right)^4, \tag{11}$$

where the "+" sign is for instanton, "−" for anti-instanton. Then at the center

$$q^{\mathrm{BPST}}(x_c) = \pm\frac{6}{\pi^2\rho^4}. \tag{12}$$

Therefore we can get the relation

$$\frac{q(x)}{q(x_c)} = \left(\frac{\rho^2}{(x-x_c)^2+\rho^2}\right)^4. \tag{13}$$

In this paper we use the peak and the 8 closest neighbor sites on the lattice to fit Eq. (13) to get the size ρ.

Like in Ref. [28], we also use 3 filter conditions to find HS caloron-like topological lumps:

(i)

$$\frac{\sqrt[4]{\frac{6}{\pi^2 q(x_c)}}}{\rho} \in (1-\epsilon_R, 1+\epsilon_R), \tag{14}$$

which comes from Eq. (12).

(ii)

$$\frac{\sum_{|x-x_c|\le a} q(x)}{\sum_{|x-x_c|\le a} s(x)} \in (1-\epsilon_S, 1+\epsilon_S), \tag{15}$$

where the normalized action density $s(x) = \frac{a^4}{8\pi^2}\sum_{\mu<\nu}\mathrm{tr}_C F^2_{\mu\nu}(x)$, the normalization factor $8\pi^2$ comes from the action of a single HS caloron $S = \frac{g^2}{\pi^2}|Q|$ with $Q = \int d^4x q(x)$.

(iii) To avoid double countings of two peaks of a single but distorted HS caloron, we filter peak $x_{c'}$ by

$$\text{if } |x_c - x_{c'}| < \epsilon\rho(x_c). \tag{16}$$

The topological lump centering at $x_{c'}$ will be filtered.

III. LOCALIZATION OF TOPOLOGICAL CHARGE DENSITY

We use the HS calorons filter conditions and IPR to investigate the localization of topological charge density. Ensembles in Table I would be used every ten configurations, which means that every ensemble includes 200 configurations and each configuration is separated by 100 sweeps. We only show the figures that result from parameters $\epsilon_R = 0.5, \epsilon_S = 0.4, \epsilon = 0.7,\ 1.0$. But we have used parameters varied in the regions $\epsilon_R = 0.3$–0.7, $\epsilon_S = 0.2 - 0.6, \epsilon = 0.7 - 1.0$. These results are consistent with the discussion in the following. We choose $\epsilon_R = 0.5$, $\epsilon_S = 0.4$ since the results are stable around them.

The gradient flow we used is of Wilson action, which means that we use Wilson flow to smear the gauge fields. The effective smearing radius λ runs from 0.3 to 0.9 fm.

In Fig. 1, we present the topological charges Q of ten configurations versus Wilson flow in every ensemble, the topological charges Q of the original configurations have also been presented. Obviously when λ runs from 0.3 to 0.9 fm, the topological charges Q approach to integers. At the same time the topological charges Q do not drop down to the value zero. Therefore the long-ranged topological structures should be preserved during the Wilson flow.

A. Investigating the HS caloron-like topological lumps

In Fig. 2, we show the three quantities of HS caloron-like topological lumps versus β: the average density $\langle N\rangle$, the average size $\langle\rho\rangle$ and $\langle q_c(x)\rangle$, which is the average absolute value of topological charge density on the peak. The three quantities with different effective smearing radius are marked with different colors or shapes.

With the increase of the effective smearing radius λ, the average density $\langle N\rangle$ decreases monotonically, the average size $\langle\rho\rangle$ grows monotonically. Unlike $\langle N\rangle$ and $\langle\rho\rangle$, $\langle q_c(x)\rangle$ of the ensembles at higher temperatures decreases at first, then becomes to increase instead as λ increases.

The phenomena that $\langle N\rangle$ decreases monotonically and $\langle\rho\rangle$ grows monotonically can be expected. Since with the increase of λ, more and more small topological lumps would be smoothed out.

When λ is large, we find that the three quantities of HS caloron-like topological lumps are consistent at $\beta = 6.045$

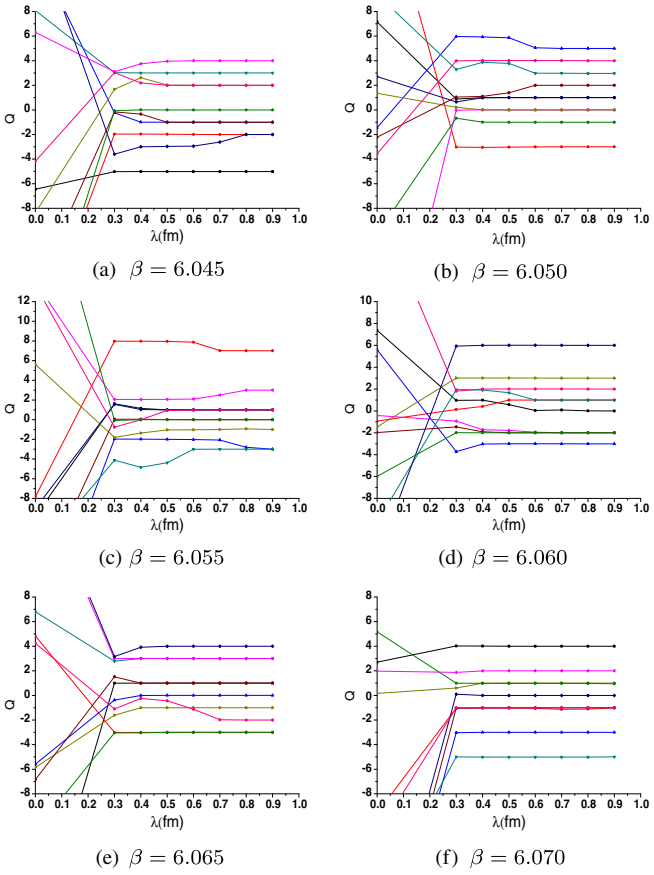

(a) $\beta = 6.045$ (b) $\beta = 6.050$ (c) $\beta = 6.055$ (d) $\beta = 6.060$ (e) $\beta = 6.065$ (f) $\beta = 6.070$

FIG. 1. The topological charges Q of ten configurations versus Wilson flow, λ runs from 0.3 to 0.9 fm. Q of original configurations have also been presented. The topological charges approach to integers and do not drop down to the value zero during the Wilson flow.

and $\beta = 6.050$. It indicates that the localization of topological charge density is stable. When $\beta \geq 6.055$, we find that the three quantities change significantly as the temperature increases. It means that the topological structures have a transition point near $\beta = 6.055$.

Since when λ is small, the short-ranged fluctuations may not be suppressed enough, we need not pay much attention to the behaviors of the three quantities of the HS caloron-like topological lumps at small λ.

The decrease of the average density $\langle N \rangle$ when $\beta \geq 6.055$ means that the topological excitation is suppressed. It may explain why the topological susceptibility starts to drop down near T_c [29].

Noting that $\frac{1}{\langle N \rangle}$, the average volume occupied by one HS caloron-like topological lump, is always close to $(2\langle \rho \rangle)^4$, the average volume of the HS caloron-like topological lumps. It means that the HS caloron-like topological lumps are not sparse but dense.

Since the chiral condensate $\langle \bar{\psi}\psi \rangle \propto -\frac{\langle N \rangle^{\frac{1}{2}}}{\langle \rho \rangle}$ [5], the decrease of $\langle N \rangle$ and the increase of $\langle \rho \rangle$ as the temperature increases at $\beta \geq 6.055$ indicate that the absolute value of chiral condensate will drop down as the temperature rises. It is consistent with the fact that the chiral symmetry will restore at high temperature.

IPR has also been used to study the localization of $q(x)$, and conclusions from both methods are consistent.

B. Average IPR versus β with Wilson flow

In Fig. 3 we show the average inverse participation ratio $\langle \mathrm{IPR} \rangle$ versus β with Wilson flow. Theoretically, when a certain structure is embedded in a finite $4D$ space discretized by lattice spacing a, the IPR of the structure obeys $\mathrm{IPR} \sim a^{4-d}$ as $a \to 0$ [22], where d denotes the dimension of the structure. But the dependence of IPR on the volume of the finite $4D$ space is small [22]. However, when we use gradient flow to smear the configurations in a space discretized with different lattice spacings, the average IPR of $q(x)$ with same λ would be almost the same if λ is large enough, only mild scaling violation is found [23]. Therefore, any manifest differences of $\langle \mathrm{IPR} \rangle$ of $q(x)$ among different temperatures cannot result from the lattice discretization with different lattice spacings. The manifest differences can only result from the different localizations of topological charge density at different temperatures.

In Fig. 3 we find that when λ is large, $\langle \mathrm{IPR} \rangle$ increases as β increases when $\beta \geq 6.055$. It is just the same transition point that we found in Sec. III A. Obviously, this behavior of $\langle \mathrm{IPR} \rangle$ should come from the fact that the topological localization was enhanced by the increase of temperature. The ensembles at $\beta = 6.045$ and $\beta = 6.050$ have $\langle \mathrm{IPR} \rangle$ compatible for all used λ. It means that the localization of $q(x)$ has not changed yet when $\beta \leq 6.050$, just like the behaviors of the three quantities of HS caloron-like topological lumps in Fig. 2.

By using the two different methods, we get the conclusion that the localization of topological charge density near T_c does not change when $\beta \leq 6.050$, and starts to change significantly when $\beta \geq 6.055$.

IV. EXTRACTING THE PSEUDOSCALAR GLUEBALL MASS FROM THE TCDC AT HIGH TEMPERATURE

The topological charge density correlator (TCDC) is defined by

$$C_{qq}(r) = \langle q(x)q(y) \rangle, \quad r = |x - y|. \tag{17}$$

In the negative tail region of the TCDC, it can be approximated by the pseudoscalar propagator [30]

$$\langle q(x)q(y) \rangle = \frac{m}{4\pi^2 r} K_1(mr), \quad r = |x - y|,$$

where $K_1(z)$ is the modified Bessel function, it has the asymptotic form as

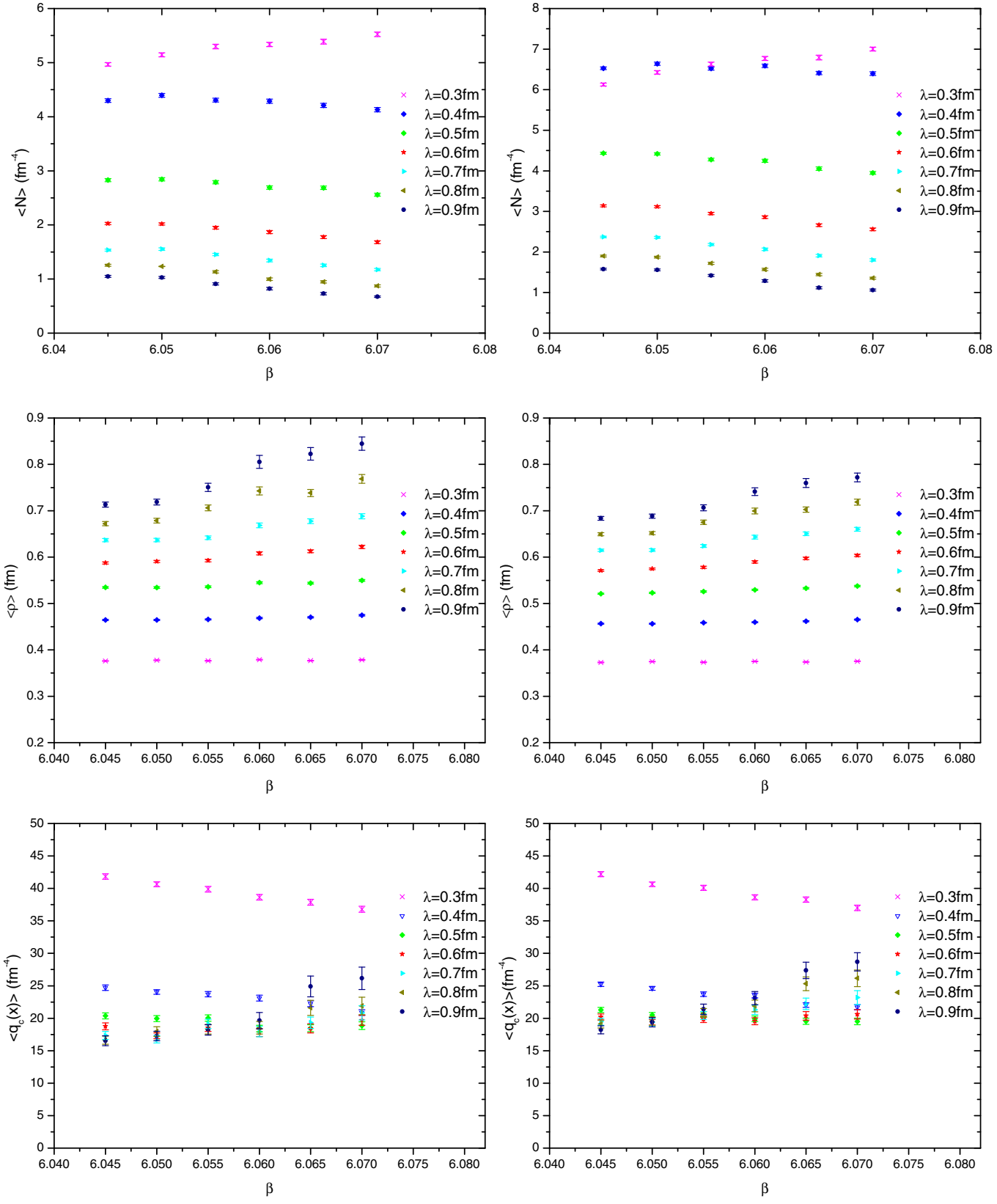

FIG. 2. The parameters setting: $\epsilon_R = 0.5$, $\epsilon_S = 0.4$, left panels: $\epsilon = 1.0$, right panels: $\epsilon = 0.7$. From top to bottom: the average density $\langle N \rangle$, the average size $\langle \rho \rangle$, and the average absolute value $\langle q_c(x) \rangle$.

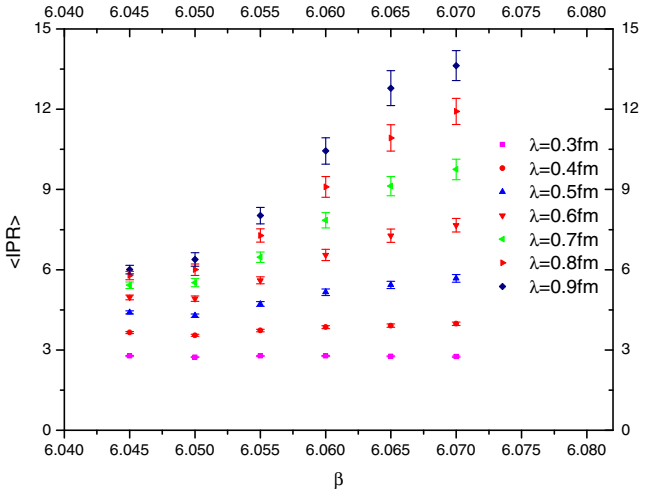

FIG. 3. ⟨IPR⟩ of topological charge density with Wilson flow versus the inverse coupling β, the effective smearing radius λ of Wilson flow runs from 0.3 to 0.9 fm.

$$K_1(z) \underset{\text{large } z}{\sim} e^{-z}\sqrt{\frac{\pi}{2z}}\left[1+\frac{3}{8z}\right]. \tag{18}$$

Thus we can extract the mass of pseudoscalar particle by fitting Eq. (18) at zero temperature [23,31,32].

We may also use Eq. (18) to extract the pseudoscalar glueball mass from TCDC at finite temperature in quenched lattice QCD, the mass m and amplitude are set to be two free parameters in the fitting procedure. The procedure has been applied to the two ensembles in Table II. The effective smearing radius λ of Wilson flow runs from 0.12 to 0.20 fm, each ensemble includes 500 configurations.

We find that when the starting point of the fitting range is fixed and the ending point is varied, once the error bar of the TCDC at the ending point touches the value zero, the fitting result is independent of the ending point. This phenomenon is also found in Ref. [23]. Therefore we fix the ending point that the error bar of the TCDC has touched the value zero and vary the starting point to extract preliminary pseudoscalar glueball mass M. Then we find the proper λ and fitting window to extract the final pseudoscalar glueball mass M. Results are showed in Fig. 4.

TABLE II. The quenched ensembles of Wilson action in this work. The lattice size is $32^3 \times 8$. 10000 sweeps were done before thermalization. Each configuration is separated by 100 sweeps. Each sweep includes 5 times quasi heat-bath and 5 steps of leapfrog.

β	6.170	6.236
N_{cnfg}	500	500
T	$1.19T_c$	$1.36T_c$

Both ensembles have the most stable plateau of the preliminary pseudoscalar glueball mass M at $\lambda = 0.16$ fm. Therefore we choose the data from $\lambda = 0.16$ fm to extract M. The final fitting window is determined by the range that the plateaus of the preliminary pseudoscalar glueball mass overlap with plateaus nearby. In Fig. 4, red solid lines denote the final fitting results of the pseudoscalar glueball mass M, their ranges represent the final fitting windows, pink dash lines represent the errors of the final pseudoscalar glueball mass M. Numeric results are $T = 1.19T_c$, $M = 1.915(98) \times 10^3$ MeV and $T = 1.36T_c$, $M = 1.829(123) \times 10^3$ MeV. For comparing our results with those from Ref. [24], we had used same parameter $r_0 \approx 410$ MeV as Ref. [24] does. The fitting results are consistent with those from Ref. [24]. Noting that the final fitting window in the left panel is shorter than that in the right panel. It should be owing to the coarser lattice spacing a of the ensemble in the left panel, same thing has also been found in Ref. [23]. In fact, we also apply the fitting procedure to ensembles at

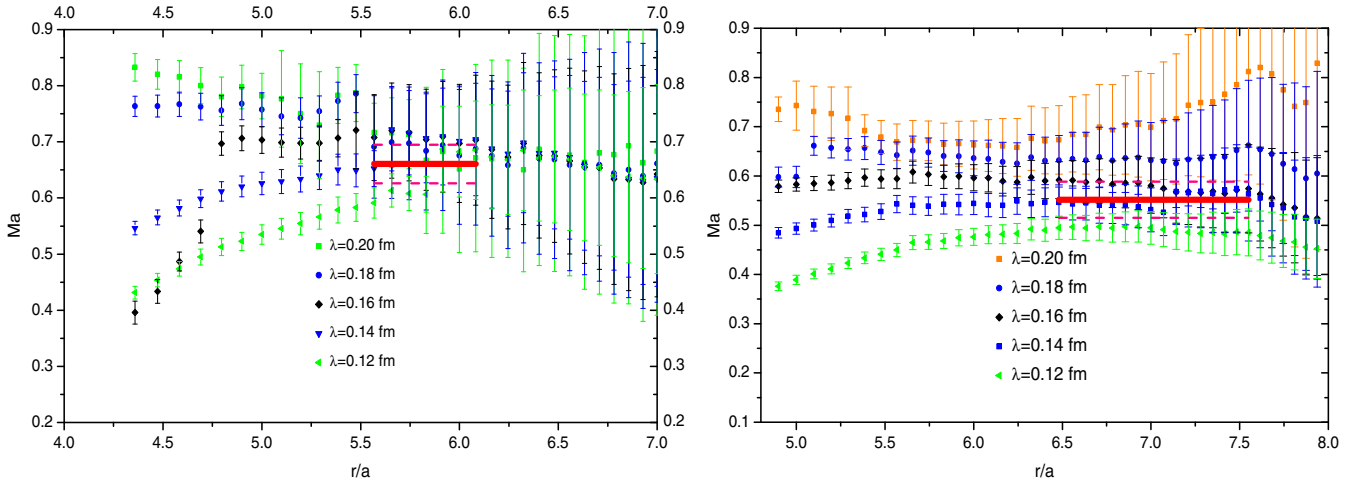

FIG. 4. The pseudoscalar glueball mass M with Wilson flow and fixed ending point, the horizontal axis r/a is the starting point of the preliminary fitting range. Left: $T = 1.19T_c$, right: $T = 1.36T_c$.

lower temperatures, which means ensembles with coarser lattice spacing a, but fail to get proper final fitting windows to extract the final pseudoscalar glueball mass M. As for our work, this method is available for extracting the pseudoscalar glueball mass at finite temperature with lattice spacing $a < 0.08$ fm.

V. SUMMARY

In this paper we use Wilson flow to smear ensembles of quenched lattice QCD with lattice volume $32^3 \times 8$ at finite temperature. To study the topological structure of quenched QCD vacuum near T_c corresponding to the critical inverse coupling $\beta_c = 6.06173(49)$, we have used HS caloron-like topological lumps and IPR of topological charge density. When the effective smearing radius λ is large enough, we find that the three quantities of HS caloronlike topological lumps are stable when $\beta \leq 6.050$. But these quantities change significantly when $\beta \geq 6.055$. Similar behaviour is also found by using IPR to investigate the localization of topological charge density, so the result is reliable. We extract the pseudoscalar glueball mass from TCDC at $T = 1.19T_c, 1.36T_c$, the results are consistent with those from conventional method.

ACKNOWLEDGMENTS

This work was mainly run on Tianhe-2 supercomputer at NSCC in Guangzhou. Supported in part by the National Natural Science Foundation of China (NSFC) under the project No. 11335001, No. 11275169.

[1] E. Witten, Current algebra theorems for the U(1) "Goldstone boson", Nucl. Phys. **B156**, 269 (1979).
[2] G. Veneziano, U(1) without instantons, Nucl. Phys. **B159**, 213 (1979).
[3] G. Veneziano, Goldstone mechanism from gluon dynamics, Phys. Lett. **95B**, 90 (1980).
[4] E. Witten, Instatons, the quark model, and the 1/N expansion, Nucl. Phys. **B149**, 285 (1979).
[5] D. Diakonov, Chiral symmetry breaking by instantons, arXiv:hep-ph/9602375.
[6] A. A. Belavin, A. M. Polyakov, A. S. Schwartz, and Y. S. Tyupkin, Pseudoparticle solutions of the Yang-Mills equations, Phys. Lett. **59B**, 85 (1975).
[7] T. DeGrand, A. Hasenfratz, and T. G. Kovács, Topological structure in the SU (2) vacuum, Nucl. Phys. **B505**, 417 (1997).
[8] T. DeGrand, A. Hasenfratz, and T. G. Kovács, Topological structure in the SU(2) vacuum, Nucl. Phys. B, Proc. Suppl. **63**, 528 (1998).
[9] D. Smith, H. Simma, and M. Teper, Topological structure of the SU(3) vacuum and exceptional eigenmodes of the improved Wilson-Dirac operator, Nucl. Phys. B, Proc. Suppl. **63**, 558 (1998).
[10] D. A. Smith and M. J. Teper, Topological structure of the SU(3) vacuum, Phys. Rev. D **58**, 014505 (1998).
[11] M. Feurstein, H. Markum, and S. Thurner, Visualization of topological structure and chiral condensate, Nucl. Phys. B, Proc. Suppl. **63**, 477 (1998).
[12] B. Berg, Dislocations and topological background in the lattice O(3) σ-model, Phys. Lett. **104B**, 475 (1981).
[13] M. Albanese, F. Costantini, G. Fiorentini, F. Flore, M. P. Lombardo, R. Tripiccione, P. Bacilieri, L. Fonti, P. Giacomelli, E. Remiddi, M. Bernaschi, N. Cabibbo, E. Marinari, G. Parisi, G. Salina, S. Cabasino, F. Marzano, P. Paolucci, S. Petrarca, F. Rapuano, P. Marchesini, and R. Rusack, Glueball masses and string tension in lattice QCD, Phys. Lett. B **192**, 163 (1987).
[14] A. Hasenfratz and F. Knechtli, Flavor symmetry and the static potential with hypercubic blocking, Phys. Rev. D **64**, 034504 (2001).
[15] C. Morningstar and M. Peardon, Analytic smearing of SU(3) link variables in lattice qcd, Phys. Rev. D **69**, 054501 (2004).
[16] P. J. Moran and D. B. Leinweber, Over-improved stout-link smearing, Phys. Rev. D **77**, 094501 (2008).
[17] M. Lüscher, Properties and uses of the wilson flow in lattice qcd, J. High Energy Phys. 08 (2010) 071.
[18] C. Bonati and M. D'Elia, Comparison of the gradient flow with cooling in $SU(3)$ pure gauge theory, Phys. Rev. D **89**, 105005 (2014).
[19] B. A. Berg and D. A. Clarke, Deconfinement, gradient, and cooling scales for pure SU(2) lattice gauge theory, Phys. Rev. D **95**, 094508 (2017).
[20] B. A. Berg and D. A. Clarke, Topological charge and cooling scales in pure SU(2) lattice gauge theory, Phys. Rev. D **97**, 054506 (2018).
[21] B J. Harrington and H. K. Shepard, Periodic euclidean solutions and the finite-temperature Yang-Mills gas, Phys. Rev. D **17**, 2122 (1978).
[22] C. Aubin, C. Bernard, S. Gottlieb, E. B. Gregory, U. M. Heller, J. E. Hetrick, J. Osborn, R. Sugar, D. Toussaint, w. P. de Forcrand, and O. Jahn (MILC Collaboration), The scaling dimension of low lying Dirac eigenmodes and of the topological charge density, arXiv:hep-lat/0410024.
[23] A. Chowdhury, A. Harindranath, and J. Maiti, Correlation and localization properties of topological charge density and the pseudoscalar glueball mass in SU(3) lattice Yang-Mills theory, Phys. Rev. D **91**, 074507 (2015).
[24] X.-F. Meng, G. Li, Y.-J. Zhang, Y. Chen, C. Liu, Y.-B. Liu, J.-P. Ma, and J.-B. Zhang, Glueballs at finite temperature in SU(3) Yang-Mills theory, Phys. Rev. D **80**, 114502 (2009).
[25] S. Necco and R. Sommer, The $N_f = 0$ heavy quark potential from short to intermediate distances, Nucl. Phys. **B622**, 328 (2002).

[26] R. Sommer, A new way to set the energy scale in lattice gauge theories and its application to the static force and σ_s in SU(2) Yang-Mills theory, Nucl. Phys. **B411**, 839 (1994).

[27] A. Francis, O. Kaczmarek, M. Laine, T. Neuhaus, and H. Ohno, Critical point and scale setting in SU(3) plasma: An update, Phys. Rev. D **91**, 096002 (2015).

[28] A. Athenodorou, P. Boucaud, F. De Soto, J. Rodríguez-Quintero, and S. Zafeiropoulos, Instanton liquid properties from lattice QCD, J. High Energy Phys. 02 (2018) 140.

[29] G.-Y. Xiong, J.-B. Zhang, Y. Chen, C. Liu, Y.-B. Liu, and J.-P. Ma, Topological susceptibility near T_c in SU(3) gauge theory, Phys. Lett. B **752**, 34 (2016).

[30] E. V. Shuryak and J. J. M. Verbaarschot, Screening of the topological charge in a correlated instanton vacuum, Phys. Rev. D **52**, 295 (1995).

[31] H. Fukaya, S. Aoki, G. Cossu, S. Hashimoto, T. Kaneko, and J. Noaki, η' meson mass from topological charge density correlator in QCD, Phys. Rev. D **92**, 111501 (2015).

[32] Y.-H. Zou, J.-B. Zhang, G.-Y. Xiong, Y. Chen, C. Liu, Y.-B. Liu, and J.-P. Ma, Investigating the topological structure of quenched lattice QCD with overlap fermions using a multi-probing approximation, Chin. Phys. C **41**, 103104 (2017).